J. Fluid Mech. (2015), *vol.* 769, *pp.* 621–634.
doi:10.1017/jfm.2015.143

On three-dimensional internal gravity wave beams and induced large-scale mean flows

T. Kataoka[1] **and T. R. Akylas**[2,†]

[1]Department of Mechanical Engineering, Graduate School of Engineering, Kobe University, Rokkodai, Nada, Kobe 657-8501, Japan

[2]Department of Mechanical Engineering, Massachusetts Institute of Technology, Cambridge, MA 02139, USA

(Received 12 September 2014; revised 28 January 2015; accepted 2 March 2015; first published online 25 March 2015)

The three-dimensional propagation of internal gravity wave beams in a uniformly stratified Boussinesq fluid is discussed, assuming that variations in the along-beam and transverse directions are of long length scale relative to the beam width. This situation applies, for instance, to the far-field behaviour of a wave beam generated by a horizontal line source with weak transverse dependence. In contrast to the two-dimensional case of purely along-beam variations, where nonlinear effects are minor even for beams of finite amplitude, three-dimensional nonlinear interactions trigger the transfer of energy to a circulating horizontal time-mean flow. This resonant beam–mean-flow coupling is analysed, and a system of two evolution equations is derived for the propagation of a small-amplitude beam along with the induced mean flow. This model explains the salient features of the experimental observations of Bordes *et al.* (*Phys. Fluids*, vol. 24, 2012, 086602).

Key words: geophysical and geological flows, internal waves

1. Introduction

In a recent laboratory experiment, Bordes *et al.* (2012) report observations of a strong mean flow accompanying a time-harmonic internal gravity wave beam of limited lateral extent propagating along a relatively wide stratified fluid tank. This mean flow had a jet-like structure in the beam interior and featured horizontal recirculations which extended outside the wave beam. Based on multiple-scale analysis of a modulated sinusoidal plane wave, Bordes *et al.* (2012) argued that the observed mean flow is a form of steady streaming (Lighthill 1978, § 4.7) driven by Reynolds stresses due entirely to three-dimensional effects. In the experimental set-up, three-dimensional wave variations were brought about by viscous attenuation along the beam propagation direction and by the finite extent of the wave generator in the vertical and transverse directions.

The findings of Bordes *et al.* (2012) add to growing evidence that the generation of mean flows is central to three-dimensional internal wave beam dynamics. Laboratory experiments and numerical simulations (Grisouard *et al.* 2013) of the reflection

† Email address for correspondence: trakylas@mit.edu

from a slope of a wave beam of finite extent in the transverse direction revealed a wave-induced mean flow with amplitude comparable to that of the incident wave; such a strong mean flow, though, was not observed in two-dimensional simulations, where transverse variations were absent. Moreover, according to linear stability analysis, a uniform wave beam can be unstable to long-wavelength disturbances only if such modulations vary in the along-beam and the transverse directions (Kataoka & Akylas 2013). This purely three-dimensional instability involves a resonant interaction between the underlying wave beam and a perturbation that comprises a time-harmonic component, with the beam frequency, and a mean flow.

Motivated by the works cited above, here we put forward a theoretical model for the three-dimensional propagation of small-amplitude internal wave beams in a uniformly stratified Boussinesq fluid, assuming that variations in the along-beam and transverse directions are of long length scale relative to the beam width. In the corresponding two-dimensional problem, where transverse variations are absent, nonlinear effects turn out to be minor, even for beams of finite amplitude (Tabaei & Akylas 2003). Three-dimensional variations, by contrast, enable resonant transfer of energy to the flow mean vertical vorticity, resulting in strong nonlinear coupling between a wave beam and its induced mean flow.

The key role of the vertical vorticity in three-dimensional internal waves is discussed by Lighthill (1996). Specifically, vertical vorticity, which involves the horizontal fluid motion, is conserved for linear inviscid disturbances. Thus, in three dimensions, apart from the internal wave motion which obeys the familiar dispersion relation, there is also a zero-frequency non-propagating mode associated with the mean horizontal motion. These two modes are completely uncoupled in the linear theory. However, in the case of a small-amplitude internal wave beam of interest here, the Reynolds stresses brought about by the presence of both along-beam and transverse variations resonantly force the mean vertical-vorticity mode, thus triggering the transfer of energy to a circulating horizontal mean flow.

Our analysis of this nonlinear coupling mechanism leads to a system of two nonlinear equations for the beam–mean-flow evolution in three dimensions. This relatively simple model explains the salient features of the observations of Bordes *et al.* (2012), even though the assumed separation of scales (length scale of transverse variations $\gg$ beam width) is not strictly satisfied in the experiment.

The proposed model applies to modulated internal wave beams with general locally confined profile of $O(1)$ width in the cross-beam direction. Such disturbances are distinct from nearly monochromatic wavetrains, considered in the analysis by Bordes *et al.* (2012) and several earlier mean-flow computations; see Tabaei & Akylas (2007) and references given therein. As a result, the equations governing the beam–mean-flow coupling in three dimensions are very different from the nonlinear-Schrödinger-type models obtained in prior work. Moreover, in the problem at hand, as the induced mean flow extends far from the beam vicinity, we find it necessary to follow a matched-asymptotics procedure for deriving the appropriate evolution equations.

In oceans, internal wave beams form the backbone of the internal tide, which is generated by the interaction of the barotropic tide with bottom topography. The internal tide breakdown and its potential contribution to deep-ocean mixing have attracted considerable attention. To shed light on these processes, numerous studies have focused on instabilities of internal wavetrains to subharmonic short-scale disturbances; see, for example, Staquet & Sommeria (2002), Koudella & Staquet (2006), Karimi & Akylas (2014) and references given therein. The interaction mechanism discussed here suggests that energy transfer from the internal tide to

large-scale horizontal mean flows is also possible, particularly in regions of strong three-dimensional variations, and such an 'inverse cascade' could play a part in horizontal mass and momentum transport.

This scenario is further supported by Grisouard & Bühler (2012), who computed the leading-order mean-flow response due to small-amplitude three-dimensional dissipating internal tides, also taking into account the effect of background rotation. In this more realistic oceanic setting, they also find that energy is transferred to a horizontal mean flow by a resonance mechanism, similar to the one discussed here. On the other hand, by focusing on an isolated internal wave beam with three-dimensional modulations, the ensuing analysis leads to a fully coupled model, which describes the resonant mean-flow response and also accounts for the effect of the growing mean flow on the long-time beam propagation.

2. Formulation and scalings

An inviscid uniformly stratified Boussinesq fluid supports time-harmonic plane internal gravity waves with general spatial profile. Such wave beams obey the familiar internal-wave dispersion relation of sinusoidal plane waves,

$$\omega^2 = N^2 \sin^2\theta, \tag{2.1}$$

where ω is the wave frequency, θ is the beam angle to the horizontal and N is the (constant) background buoyancy frequency.

A simple way of generating wave beams in the laboratory, as demonstrated in the early experiments of Mowbray & Rarity (1967), is by oscillating a long horizontal cylinder at a frequency $\omega < N$ in a stratified fluid tank. This type of mechanical forcing gives rise to a wave pattern known as 'St. Andrew's Cross', which comprises four beams that stretch radially outward from the cylinder along directions fixed by the dispersion relation (2.1); see, for example, Lighthill (1978, p. 314). Bordes *et al.* (2012), instead, employed a recently developed mechanical wave generator (Gostiaux *et al.* 2007; Mercier *et al.* 2010) placed at one side of a stratified fluid tank. This set-up made it possible to excite a single wave beam and also prescribe the beam profile.

The present study focuses on the far-field propagation of a three-dimensional internal wave beam, ignoring the detailed behaviour near the forcing region. For this purpose, we shall use as wave source an externally applied time-harmonic line force centred at $x = y = 0$, with x being the horizontal, y the vertical and z the transverse horizontal direction. To describe the far-field evolution of one of the four beams due to this source, it is convenient to use a rotated coordinate system, with ξ being the along-beam and η the cross-beam direction (figure 1). Moreover, we shall work with dimensionless variables, employing $1/N$ as the time scale and a characteristic length L_* associated with the applied forcing (to be specified below) as the length scale. Then, the flow-velocity components $\boldsymbol{u} = (u, v, w)$ along (ξ, η, z) and the reduced density ρ and pressure p are governed by

$$\boldsymbol{\nabla}\cdot\boldsymbol{u} = 0, \tag{2.2}$$

$$\rho_t + \boldsymbol{u}\cdot\boldsymbol{\nabla}\rho = -u\sin\theta + v\cos\theta, \tag{2.3}$$

$$u_t + \boldsymbol{u}\cdot\boldsymbol{\nabla}u = -p_\xi + \rho\sin\theta + \nu\nabla^2 u + F, \tag{2.4a}$$

$$v_t + \boldsymbol{u}\cdot\boldsymbol{\nabla}v = -p_\eta - \rho\cos\theta + \nu\nabla^2 v + H, \tag{2.4b}$$

$$w_t + \boldsymbol{u}\cdot\boldsymbol{\nabla}w = -p_z + \nu\nabla^2 w. \tag{2.4c}$$

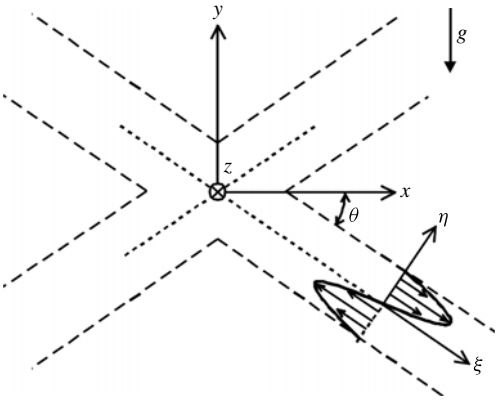

FIGURE 1. Schematic of a St. Andrew's Cross generated by an external time-harmonic line force with frequency $\omega = \sin\theta$ $(0 < \theta < \pi/2)$. The force is locally confined near $x = y = 0$ and slowly varying along z. The analysis focuses on the propagation of one of the four generated beams far from the forcing region. It is assumed that variations in the along-beam (ξ) and transverse horizontal (z) directions are weak in comparison with variations in the cross-beam (η) direction.

Here, (F, H) are the components of the applied force along (ξ, η) and $\nu = \nu_*/NL_*^2$ stands for the inverse Reynolds number, where ν_* is the kinematic viscosity.

A key assumption in the ensuing asymptotic analysis is that the external force, which is locally confined in ξ and η, varies slowly in the transverse (z) direction. Thus, identifying the characteristic length L_* with the typical extent of the wave source in the x–y plane, the force components F and H are expressed as

$$F = \alpha\left\{\hat{F}(\xi, \eta; Z)\mathrm{e}^{-\mathrm{i}\omega t} + \text{c.c.}\right\}, \quad H = \alpha\left\{\hat{H}(\xi, \eta; Z)\mathrm{e}^{-\mathrm{i}\omega t} + \text{c.c.}\right\}, \tag{2.5a,b}$$

where $\hat{F}$ and $\hat{H}$ are $O(1)$. Here,

$$Z = \varepsilon z \quad (0 < \varepsilon \ll 1) \tag{2.6}$$

is a 'stretched' transverse coordinate and $\omega = \sin\theta$ $(0 < \theta < \pi/2)$ according to (2.1) in dimensionless form. In addition, it is assumed that the forcing amplitude parameter α in (2.5) is small $(0 < \alpha \ll 1)$, so the amplitude of the generated beam is small as well.

Under these assumptions and light viscous dissipation $(\nu \ll 1)$, the response in the far field $(\xi, t \gg 1)$ is expected to be a nearly uniform wave beam, whose profile has $O(1)$ width in η but is slowly varying in the along-beam (ξ) and transverse (z) directions. Our goal is to set up a far-field asymptotic theory for beam propagation, in the 'distinguished limit' where the weak dispersion due to along-beam and transverse variations, small nonlinearity and light viscous dissipation formally carry equal weight.

Specifically, from prior experience with modulated wave beams (Tabaei & Akylas 2003; Kataoka & Akylas 2013), to make the transverse dispersion due to the dependence on $Z = \varepsilon z$ as important as along-beam dispersion, we take the scale of along-beam variations to be $O(\varepsilon^{-2})$; according to the dispersion relation (2.1), transient effects due to such modulations then evolve on a time scale of $O(\varepsilon^{-2})$. Hence, the appropriate 'stretched' along-beam coordinate and 'slow' time are

$$(X, T) = \varepsilon^2(\xi, t). \tag{2.7}$$

Turning next to viscous dissipation, from Lighthill (1978, § 4.7), the attenuation length scale for a beam of $O(1)$ width is $O(1/\nu)$. Thus, for dissipation to act on the same $O(\varepsilon^{-2})$ length scale as along-beam dispersion, it is necessary that $\nu = O(\varepsilon^2)$; thus, we write

$$\nu = \beta\varepsilon^2, \tag{2.8}$$

where $\beta = O(1)$.

Finally, it remains to link the forcing amplitude parameter α, which controls the beam nonlinearity, to the modulation parameter ε. Our earlier stability analysis of a uniform wave beam to three-dimensional modulations (Kataoka & Akylas 2013) suggests that the appropriate balance for small-amplitude beams is

$$\alpha = \varepsilon^{1/2}. \tag{2.9}$$

Under this scaling, the beam coupling with the induced mean flow, which turns out to be the dominant nonlinear interaction, comes into play on the same time scale as dispersive and viscous effects.

3. Beam–mean-flow coupling

The scalings (2.6)–(2.9) pertain to the far-field propagation of an $O(\varepsilon^{1/2})$ beam whose profile has $O(1)$ width and varies slowly along ξ and z. Accordingly, one might expect that the scaling of the beam flow variables is similar to an $O(\varepsilon^{1/2})$ modulated sinusoidal plane wave with $O(1)$ carrier wavevector along η and envelope variables $Z = \varepsilon z$, $(X, T) = \varepsilon^2(\xi, t)$; namely, $(u, \rho, p) = O(\varepsilon^{1/2})$, with the relative magnitudes of the cross-beam and transverse velocity components,

$$v = O(\varepsilon^{5/2}), \quad w = O(\varepsilon^{3/2}), \tag{3.1a,b}$$

following directly from the incompressibility condition (2.2).

It turns out, however, that these scalings hold only for strictly two-dimensional wave beams, which feature no transverse variations ($\partial/\partial Z = 0$, $w = 0$). The reason is that three-dimensional nonlinear interactions give rise to a relatively strong mean flow which in fact extends far away from the beam ($|\eta| \gg 1$) and is essential to the propagation of a beam in three dimensions. Thus, it becomes necessary to follow a matched-asymptotics procedure whereby we solve for the induced mean flow separately near and far from the beam, and then match the two solutions. As expected, different scalings are appropriate in these two flow regions. Here, we focus on the 'inner' flow, in the vicinity of the beam, $\eta = O(1)$; the 'outer' flow, far from the beam, along with matching is discussed in § 4.

With the benefit of hindsight from our stability analysis of a uniform beam where a similar complication was encountered (Kataoka & Akylas 2013), in order for inner–outer-flow matching to be possible, it is necessary to allow for an $O(\varepsilon^2)$ mean-flow component, $\varepsilon^2\overline{V}_\infty(X, Z, T)$, in the cross-beam velocity in (3.1). Thus, the proper inner scalings of $\boldsymbol{u}$, ρ and p are

$$(u, \rho, p) \to \varepsilon^{1/2}(u, \rho, p), \quad v \to \varepsilon^2\overline{V}_\infty + \varepsilon^{5/2}v, \quad w \to \varepsilon^{3/2}w. \tag{3.2a–c}$$

It should be noted that $\overline{V}_\infty$, which is independent of η, derives from nonlinear interactions due entirely to three-dimensional variations and will be determined by inner–outer-flow matching in § 4, along with the rest of the inner mean-flow components. As a whole, this induced mean flow turns out to be purely horizontal to leading order (see (4.4) below), in line with the beam–vertical-vorticity nonlinear interaction suggested in § 1.

Upon implementing (2.5)–(2.9) and (3.2), it follows from the governing equations (2.2)–(2.4), after eliminating ρ and p, that $\boldsymbol{u} = (u, v, w)$ satisfy

$$u_X + v_\eta + w_Z = 0, \tag{3.3a}$$

$$\begin{aligned} u_{tt} + u\sin^2\theta = {} & \varepsilon^{3/2}\overline{V}_\infty \sin\theta\cos\theta + \varepsilon^2\left\{v\sin\theta\cos\theta + \left(-2u_T - 2\overline{V}_\infty u_\eta \right.\right. \\ & \left.\left. + \cot\theta\int^\eta u_{tX}\mathrm{d}\eta' + \beta u_{\eta\eta}\right)_t\right\} \\ & - 2\varepsilon^2\sin\theta\delta(X)\left\{\mathrm{i}f\mathrm{e}^{-\mathrm{i}\omega t} + \mathrm{c.c.}\right\} + O(\varepsilon^{5/2}), \end{aligned} \tag{3.3b}$$

$$\begin{aligned} \left(w_\eta\sin\theta - u_Z\cos\theta\right)_t = {} & \varepsilon^2\left\{\left(u_T + \overline{V}_\infty u_\eta - \cot\theta\int^\eta u_{tX}\mathrm{d}\eta' - \beta u_{\eta\eta}\right)_Z\cos\theta \right. \\ & \left. + v_{Zt}\sin\theta - \left(w_T + \overline{V}_\infty w_\eta - \beta w_{\eta\eta}\right)_\eta\sin\theta\right\} \\ & - 2\varepsilon^2\delta(X)\left\{(f_Z\cos\theta + h_Z\sin\theta)\mathrm{e}^{-\mathrm{i}\omega t} + \mathrm{c.c.}\right\} \\ & + \varepsilon^{5/2}\left\{(\boldsymbol{u}\cdot\widehat{\boldsymbol{\nabla}}u)_Z\cos\theta - (\boldsymbol{u}\cdot\widehat{\boldsymbol{\nabla}}w)_\eta\sin\theta\right\} + O(\varepsilon^{7/2}). \end{aligned} \tag{3.3c}$$

Here, $\widehat{\boldsymbol{\nabla}} = (\partial/\partial X, \partial/\partial\eta, \partial/\partial Z)$ and, in view of (2.7) and (2.9), the external force components (2.5) have been approximated in the far field ($X, T = O(1)$) by

$$F \to 2\varepsilon^{5/2}\delta(X)\left\{f(\eta, Z)\mathrm{e}^{-\mathrm{i}\omega t} + \mathrm{c.c.}\right\}, \quad H \to 2\varepsilon^{5/2}\delta(X)\left\{h(\eta, Z)\mathrm{e}^{-\mathrm{i}\omega t} + \mathrm{c.c.}\right\}, \tag{3.4a,b}$$

where $f(\eta, Z)$ and $h(\eta, Z)$ are $O(1)$ locally confined functions in η, and $\delta(X)$ denotes the delta function.

In the two-dimensional case where transverse variations are absent ($\partial/\partial Z = 0$, $w = 0$), the inner flow equations (3.3) reduce to (3.3*a*,*b*); thus, the three-dimensional nature of the flow is reflected mainly in (3.3*c*), which governs the evolution of the vertical vorticity

$$\Omega = w_\eta\sin\theta - u_Z\cos\theta + O(\varepsilon^2). \tag{3.5}$$

Moreover, as emphasized by Lighthill (1996), if nonlinear, viscous and forcing effects are ignored, Ω is conserved according to (3.3*c*); as a result, in three dimensions, there is a zero-frequency linear mode associated with the mean vertical vorticity.

The leading-order response according to (3.3) is a wave beam with time-harmonic dependence ($u \propto \mathrm{e}^{\pm\mathrm{i}\omega t}$) at the forcing frequency $\omega = \sin\theta$. At higher order, one would expect nonlinear interactions due to along-beam and transverse variations to give rise to a mean flow (independent of t) and higher-harmonic oscillations in t ($\propto \mathrm{e}^{\pm\mathrm{i}n\omega t}$, $n > 1$). However, by virtue of (3.3*c*), the Reynolds stresses brought about by three-dimensional variations resonantly force the flow mean vertical vorticity, which is a non-propagating natural mode as remarked above; thus, the induced mean flow dominates over the rest of the harmonics.

To describe this resonant primary-harmonic–mean-flow interaction, $\boldsymbol{u}$ is expanded as follows:

$$u = \left\{U(X, \eta, Z, T)\mathrm{e}^{-\mathrm{i}\omega t} + \mathrm{c.c.}\right\} + \varepsilon^{3/2}\overline{U}(X, \eta, Z, T) + \cdots, \tag{3.6a}$$

$$v = \left\{V(X, \eta, Z, T)\mathrm{e}^{-\mathrm{i}\omega t} + \mathrm{c.c.}\right\} + \varepsilon^{1/2}\overline{V}(X, \eta, Z, T) + \cdots, \tag{3.6b}$$

$$w = \left\{W(X, \eta, Z, T)\mathrm{e}^{-\mathrm{i}\omega t} + \mathrm{c.c.}\right\} + \varepsilon^{1/2}\overline{W}(X, \eta, Z, T) + \cdots. \tag{3.6c}$$

The equations governing the amplitudes of the primary and mean harmonics in (3.6) are obtained by inserting these expansions into (3.3) and collecting the various contributions to each harmonic. Specifically, from the primary-harmonic terms in (3.3*c*) and (3.3*a*), we find

$$W = \cot\theta \int^{\eta} U_Z \mathrm{d}\eta' + O(\varepsilon^2), \tag{3.7}$$

$$V = -\int^{\eta} U_X \mathrm{d}\eta' - \cot\theta \int^{\eta} \int^{\eta'} U_{ZZ} \mathrm{d}\eta'' \mathrm{d}\eta' + O(\varepsilon^2). \tag{3.8}$$

Then, collecting primary-harmonic terms in (3.3*b*) and making use of (3.7) and (3.8) yields an evolution equation for U:

$$U_T + \overline{V}_\infty U_\eta + \mathrm{i}\cos\theta \left(\int^{\eta} U_X \mathrm{d}\eta' + \frac{\cot\theta}{2} \int^{\eta} \int^{\eta'} U_{ZZ} \mathrm{d}\eta'' \mathrm{d}\eta' \right) - \frac{\beta}{2} U_{\eta\eta} = \delta(X) f. \tag{3.9}$$

Turning next to mean terms, from (3.3*c*), after further use of (3.7) and (3.8), it follows that

$$\begin{aligned} \sin\theta \left(\overline{W}_T + \overline{V}_\infty \overline{W}_\eta - \beta \overline{W}_{\eta\eta} \right)_\eta = 2\cos\theta \Bigg\{ \left(U_Z^* \frac{\partial}{\partial \eta} - U_\eta^* \frac{\partial}{\partial Z} \right) \Bigg(\int^{\eta} U_X \mathrm{d}\eta' \\ + \frac{\cot\theta}{2} \int^{\eta} \int^{\eta'} U_{ZZ} \mathrm{d}\eta'' \mathrm{d}\eta' \Bigg) + \text{c.c.} \Bigg\}, \end{aligned} \tag{3.10}$$

where $*$ denotes complex conjugate. It should be noted that, in view of (3.6), the flow vertical vorticity (3.5) is given by

$$\Omega = \left\{ \left(W_\eta \sin\theta - U_Z \cos\theta \right) \mathrm{e}^{-\mathrm{i}\omega t} + \text{c.c.} \right\} + \varepsilon^{1/2} \overline{W}_\eta \sin\theta + O(\varepsilon^{3/2}). \tag{3.11}$$

Thus, (3.10) governs the evolution of the generated mean vertical vorticity $\overline{\Omega} = \sin\theta \overline{W}_\eta$. It should be noted that, according to the right-hand side of (3.10), $\overline{\Omega}$ is produced solely by three-dimensional nonlinear interactions – the action of the so-called Reynolds stresses brought about by longitudinal (X) and transverse (Z) variations of the wave beam.

According to the evolution equations (3.9) and (3.10), in the inner-flow region ($\eta = O(1)$), the feedback of the induced mean flow to the beam propagation is relayed via the cross-beam velocity component $\overline{V}_\infty$, which remains undetermined. To find $\overline{V}_\infty$ and thus obtain a closed system of evolution equations, we next discuss the outer flow, far from the vicinity of the beam ($|\eta| \gg 1$).

4. Outer flow and matching

Given that the forcing (3.4) is locally confined in η, the generated disturbance is expected to decay as $\eta \to \pm\infty$:

$$(\boldsymbol{u}, \rho, p) \to 0 \quad (\eta \to \pm\infty). \tag{4.1}$$

Attention is now focused on meeting these boundary conditions. To this end, we shall require that

$$\int^{\eta} \int^{\eta'} U \mathrm{d}\eta'' \mathrm{d}\eta' \to 0 \quad (\eta \to \pm\infty); \tag{4.2}$$

in view of (3.7) and (3.8), this ensures that the wave beam, described by the primary-harmonic terms in (3.6), is locally confined in the cross-beam direction, in accordance with (4.1).

In regard to the induced mean flow, however, the boundary conditions (4.1) cannot be met by the inner-flow response. Apart from $\overline{V}_\infty$ which is constant along η, (3.10) suggests that $\overline{W}$ also remains non-zero far from the beam:

$$\overline{W} \to \overline{W}_{\pm\infty}(X, Z, T) \quad (|\eta| \gg 1). \tag{4.3}$$

In addition, according to (3.6) and (3.3*b*),

$$\overline{U} = \cot\theta\, \overline{V}_\infty + O(\varepsilon^{1/2}), \tag{4.4}$$

confirming that the induced inner mean flow is purely horizontal, to leading order. Finally, upon combining (3.6) and (4.3) with (3.3*a*), it follows that

$$\overline{V} \sim -\eta \frac{\partial \overline{W}_{\pm\infty}}{\partial Z} \quad (|\eta| \gg 1). \tag{4.5}$$

Thus, from (4.3)–(4.5), accounting for the scalings (3.2) and the form of the inner expansions (3.6) introduced earlier, the asymptotic behaviour of the induced mean flow far from the beam is

$$\boldsymbol{u} \sim \varepsilon^2 \left\{ \left(\cot\theta \overline{V}_\infty, \overline{V}_\infty, \overline{W}_{\pm\infty} \right) + O(\varepsilon\eta) \right\} \quad (|\eta| \gg 1). \tag{4.6}$$

The above outer limit of the inner solution for $\boldsymbol{u}$ then suggests an outer solution in the form

$$\boldsymbol{u} = \varepsilon^2 \widetilde{\boldsymbol{U}}(X, Y, Z, T) = \varepsilon^2 (\widetilde{U}, \widetilde{V}, \widetilde{W}), \tag{4.7}$$

with $\rho = O(\varepsilon^4)$ and $p = O(\varepsilon^3)$. Here, $Y = \varepsilon\eta$ is a 'stretched' cross-beam coordinate appropriate in the outer-flow region $\varepsilon\eta = O(1)$, where the inner solution breaks down according to (4.6).

Upon substituting (4.7) into the governing equations (2.2)–(2.4), to leading order, the outer solutions for the induced mean flow, consistent with the boundary conditions (4.1), are

$$\widetilde{\boldsymbol{U}} = \int_0^\infty \left(\cot\theta,\ 1,\ \mp\frac{\mathrm{i}}{\sin\theta} \right) \widehat{V}_\infty \exp\left\{ m \left(\mathrm{i}Z \mp \frac{Y}{\sin\theta} \right) \right\} \mathrm{d}m + \text{c.c.} \quad (Y \gtrless 0). \tag{4.8}$$

Here, $\widehat{V}_\infty(X, T; m)$ denotes the Fourier transform of $\overline{V}_\infty$ with respect to Z,

$$\widehat{V}_\infty = \frac{1}{2\pi} \int_{-\infty}^{\infty} \overline{V}_\infty \mathrm{e}^{-\mathrm{i}mZ} \mathrm{d}Z. \tag{4.9}$$

Hence, matching of the outer solution (4.7) and (4.8) as $Y \to 0^\pm$ with the outer limit of the inner solution (4.6) requires that

$$\overline{W}_{\pm\infty} = \mp\frac{1}{\sin\theta} \mathscr{H}\left[\overline{V}_\infty \right], \tag{4.10}$$

where

$$\mathscr{H}\left[\overline{V}_\infty \right] = \int_{-\infty}^{\infty} \mathrm{i}\,\mathrm{sgn}(m) \widehat{V}_\infty \mathrm{e}^{\mathrm{i}mZ} \mathrm{d}m \tag{4.11}$$

denotes the Hilbert transform with respect to Z. It should be noted that, since $\widetilde{U}/\widetilde{V} = \cot\theta$ in (4.8), the outer mean flow also is purely horizontal, as expected.

Returning now to (3.10) for the inner mean vertical vorticity $\overline{W}_\eta \sin\theta$, (4.10) serve as matching conditions with the outer flow. However, upon integrating (3.10) over the whole range $-\infty < \eta < \infty$ and using these conditions, we can eliminate $\overline{W}$ and obtain an evolution equation for the cross-beam mean flow $\overline{V}_\infty(X, Z, T)$:

$$\frac{\partial \overline{V}_\infty}{\partial T} = \cos\theta \frac{\partial}{\partial Z} \mathscr{H}\left[\int_{-\infty}^{\infty} U^* \left(U_X + \frac{\cot\theta}{2} \int^{\eta} U_{ZZ} \mathrm{d}\eta'\right) \mathrm{d}\eta\right] + \text{c.c.} \tag{4.12}$$

Combined with (3.9), (4.12) thus constitutes a closed system of evolution equations for the three-dimensional propagation of a beam and the associated large-scale mean flow. Once $\overline{V}_\infty$ is known, the induced mean flow far from the beam can be readily obtained from the outer solution (4.7) and (4.8).

From the right-hand side of (4.12), it is clear that transverse (Z) variations of the beam profile U are essential to mean-flow generation. The first term, in particular, which involves both Z and X derivatives, is analogous to the mean-flow production term found by Bordes *et al.* (2012); however, our analysis reveals an additional term which derives from purely transverse variations.

Finally, making use of (3.9), the evolution equation (4.12) may be written in the alternate form

$$\frac{\partial \overline{V}_\infty}{\partial T} = \mathrm{i} \frac{\partial}{\partial Z} \mathscr{H}\left[\int_{-\infty}^{\infty} \left\{\left(U^* U_\eta\right)_T + \beta U_\eta^* U_{\eta\eta}\right\} \mathrm{d}\eta\right]. \tag{4.13}$$

This brings out the role of viscous attenuation of a wave beam in the mean-flow generation process (Lighthill 1978, § 4.7). Assuming a quasi-steady three-dimensional beam, in particular, the term proportional to the viscous parameter β on the right-hand side of (4.13) gives rise to a mean flow that grows linearly with time. The same type of secular behaviour was also found by Grisouard & Bühler (2012) for the resonant mean-flow response to dissipating three-dimensional internal tides. However, as the mean flow keeps growing, its coupling to the underlying beam reflected in (3.9) eventually comes into play, and the beam–mean-flow evolution is governed by the full system of equations (3.9) and (4.12) or (4.13).

5. Comparison with Bordes *et al.* (2012)

We now apply the asymptotic model developed above to the laboratory experiment of Bordes *et al.* (2012). Their experimental set-up used as forcing a mechanical wave-beam generator (Gostiaux *et al.* 2007; Mercier *et al.* 2010) placed at one end of a 120 cm long, 80 cm wide and 42.5 cm deep stratified fluid tank. The wave generator featured a sinusoidal profile along the vertical, with wavelength $\lambda = 3.8$ cm, and had fixed height 3λ and transverse width 3.7λ. As the ratio of vertical to lateral extent of the forcing is about 0.8, the thin-beam approximation (transverse length scale $\gg$ beam width) made in the analysis is not strictly justified in the experiment of Bordes *et al.* (2012). Nevertheless, the evolution equations (3.9) and (4.13) describe qualitatively the salient features of their observations, as discussed below.

Here, we shall report results for one of the two forcing frequencies, $\omega = \sin\theta = 0.26$, considered in the experiment. With λ as our characteristic length scale L_*, the dimensionless height of the wave generator is 3, and we select ε so that the transverse width of the wave generator is normalized to unity (in terms of Z); this choice, in

view of (2.6), specifies $\varepsilon = 0.27$. Moreover, the experimental value of the buoyancy frequency $N = 0.85$ rad s^{-1} fixes the characteristic time scale $1/N$, and with $\nu_* = 1$ mm^2 s^{-1} for the kinematic viscosity, the viscous parameter in (2.8) turns out to be $\beta = 0.011$. Unlike the formal assumptions made in the asymptotic theory, ε is actually not all that small and β is very different from 1 in the experiment.

In line with the scalings above and the sinusoidal profile of the wave generator, the forcing function $f(\eta, Z)$ on the right-hand side of (3.9) is taken in the form

$$f(\eta, Z) = \begin{cases} A_0\, \mathrm{e}^{2\pi \mathrm{i}\eta} & (-1.5 < \eta < 1.5,\ -0.5 < Z < 0.5), \\ 0 & (\text{otherwise}), \end{cases} \tag{5.1}$$

with $A_0 = 0.005$. This value was chosen such that the (dimensional) maximum amplitude of the along-tank (x) velocity component of the computed beam matches the experimentally observed value of approximately 1 mm s^{-1} (see figure 2*a* of Bordes *et al.* 2012).

The evolution equations (3.9) and (4.13) subject to the boundary conditions (4.2) were solved numerically starting from rest, $U = \overline{V}_\infty = 0$ ($T = 0$). The numerical method employed pseudo-spectral discretization in space combined with fourth-order Runge–Kutta time stepping. In applying numerically the forcing term in (3.9), it was convenient to replace $f(\eta, Z)$ in (5.1) with

$$\frac{A_0}{2}\mathrm{e}^{2\pi \mathrm{i}\eta}\,\{\tanh[5(Z+0.5)] - \tanh[5(Z-0.5)]\} \quad (-1.5 < \eta < 1.5,\ -\infty < Z < \infty), \tag{5.2}$$

and to approximate $\delta(X) \simeq (30/\sqrt{\pi})\exp\{-(30X)^2\}$. Computations were carried out in the domain $(-1.5 < X < 1.5,\ -6 < \eta < 6,\ -3 < Z < 3)$ using $256 \times 128 \times 128$ Fourier modes, which ensured sufficient spatial resolution, and time step $\Delta T = 8 \times 10^{-5}$.

Figure 2 shows side and top views of the computed x velocity component of the wave beam and induced mean flow at $T = 6$, corresponding to the dimensional time $t = 96$ s; by this time the beam amplitude U has reached a quasi-steady state for $0 < x < 40$ cm along the tank. The plots in figure 2 are in terms of dimensional variables and the colour code has been chosen so as to facilitate direct comparison with the corresponding experimental results displayed in figure 2 of Bordes *et al.* (2012). (It should be noted that Bordes *et al.* (2012) do not report how long after the wave generator was turned on their results were obtained; also, they use z for the vertical and y for the transverse horizontal coordinate.) In computing the x component of the mean flow plotted in figure 2(*c*,*d*), we have combined the leading-order inner-flow solution (4.4) in the vicinity of the beam ($-1.5 \lesssim \eta \lesssim 1.5$) with the outer-flow solutions (4.7) and (4.8) away from the beam. It should be noted that, as the separation of scales assumed in the analysis (beam width $\ll$ transverse length scale) is not actually satisfied in the experiment, the extent of the inner region is comparable to that of the outer regions.

The theoretical predictions for both the beam and the induced mean flow are in qualitative agreement with the observations. Specifically, in regard to the induced mean flow, the vertical flow slice at the centre ($z = 0$) of the wavemaker (figure 2*c*) shows a strong jet-like mean flow inside the beam near the wavemaker, consistent with figure 2(*c*) of Bordes *et al.* (2012). It should be noted that this jet-like structure is clearly brought out by the asymptotic analysis: according to (4.4), the inner mean flow is horizontal and the x component remains constant across the beam since $\overline{V}_\infty$ is independent of η. Moreover, the horizontal flow slice at the mid-depth ($y = 21.6$ cm)

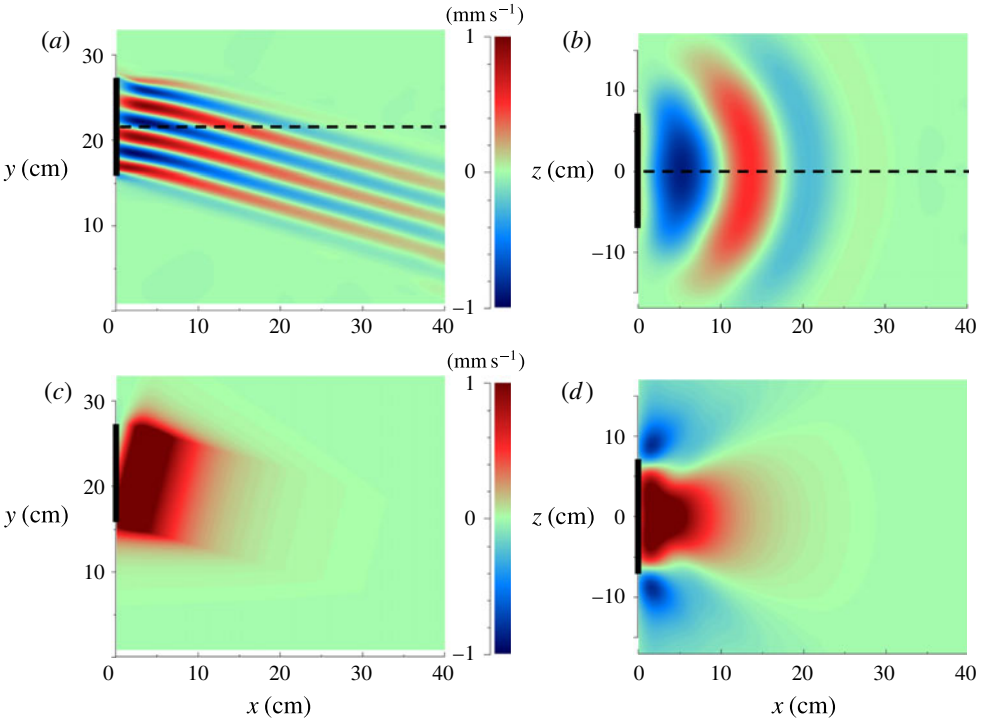

FIGURE 2. (Colour online) Computed (dimensional) x velocity component of the wave beam (a,b) and induced mean flow (c,d) at $T = 6$ (dimensional $t = 96$ s). The plots are prepared so as to facilitate direct comparison with the experimental results in figure 2 of Bordes *et al.* (2012). (It should be noted that they use z for the vertical and y for the transverse horizontal coordinate.) The location of the wavemaker is shown in black. (a,c) Vertical flow slice at the centre ($z = 0$) of the wavemaker; (b,d) horizontal flow slice at the mid-depth ($y = 21.6$ cm) of the wavemaker.

of the wave generator (figure 2*d*) confirms that the mean-flow recirculations extend outside the wave beam, as also indicated by figures 1(*b*) and 2(*d*) of Bordes *et al.* (2012).

Turning next to the computed wave beam, the wave crests are attenuated along the propagation direction due to viscous dissipation (figure 2*a*) and are also spread in the transverse direction due to dispersion (figure 2*b*), in agreement with the experimental observations (see figure 2*b* of Bordes *et al.* 2012). Further, the beam crests are noticeably bent in the transverse direction (figure 2*b*), consistent with figure 2(*b*) of Bordes *et al.* (2012) as well. Apart from the effect of transverse dispersion, this transverse bending is also caused by the coupling of the beam to the induced mean flow. It should be noted that, according to (3.9), the beam amplitude U is convected in the cross-beam direction η by the cross-beam mean-flow component $\overline{V}_\infty(X, Z, T)$; however, as $\overline{V}_\infty$ varies in Z, this convection is non-uniform, resulting in bending of the crests in the transverse direction.

To further clarify the effect of the induced mean flow on the beam propagation, figure 3 shows vertical and horizontal slices of the wave beam as in figure 2(*a*,*b*), but for the linear response, computed by setting $\overline{V}_\infty = 0$ in (3.9). Upon comparing figure 3(*b*) with 2(*b*), it is clear that the beam crests suffer less transverse bending

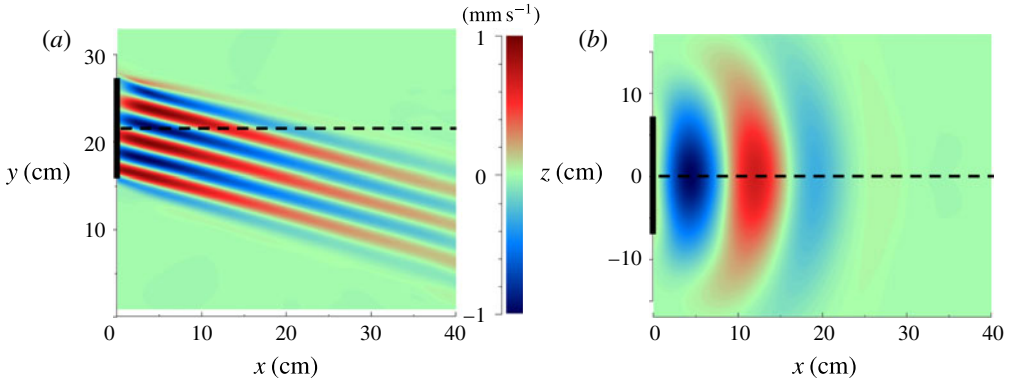

FIGURE 3. (Colour online) Computed (dimensional) x velocity component of the wave beam at $T = 6$ (dimensional $t = 96$ s), based on the linear version of (3.9) ignoring the induced mean flow ($\overline{V}_\infty = 0$). The location of the wavemaker is shown in black. (a) Vertical flow slice at the centre ($z = 0$) of the wavemaker; (b) horizontal flow slice at the mid-depth ($y = 21.6$ cm) of the wavemaker.

when the mean flow is ignored; moreover, the nonlinear response (figure 2b) is in closer agreement with the experimental observations shown in figure 2(b) of Bordes *et al.* (2012). In addition, since $\overline{V}_\infty$ also varies in X, a slight bending of the beam crests can be detected in the along-beam direction as well, as indicated by the vertical flow slice in our figure 2(a) and that of Bordes *et al.* (2012); the crests of the corresponding linear response, by contrast, are straight (figure 3a).

Bordes *et al.* (2012) also discuss the temporal evolution of the vertical vorticity associated with the observed mean flow. Specifically, they report results for $I(t)$, the integrated mean vertical vorticity over the horizontal quarter plane $0 < x < \infty$, $0 < z < \infty$ at the mid-depth of the wave generator ($y = 21.6$ cm). Theoretically, since the outer flow is irrotational, $I(t)$ (in dimensional form) can be computed asymptotically from the inner-flow solution as

$$I \sim \varepsilon L_*^2 N \int_0^\infty \int_0^\infty \sin\theta \overline{W}_\eta|_{X=0} \frac{\mathrm{d}\eta}{\sin\theta} \mathrm{d}Z$$
$$= \varepsilon L_*^2 N \int_0^\infty \overline{W}_\infty|_{X=0} \mathrm{d}Z, \tag{5.3}$$

where $\overline{W}_\infty$ is given in terms of $\overline{V}_\infty$ by (4.10). For computation purposes, $\overline{W}_\infty|_{X=0}$ in (5.3) was replaced by the average value of $\overline{W}_\infty$ over the region $0 < X < 1.5\varepsilon^2 \cot\theta$, where the inner flow intersects with $y = 21.6$ cm. Figure 4 shows a comparison of computed values of $I(t)$ based on (5.3) against experimental results from figure 4(a) of Bordes *et al.* (2012) for the induced mean flow obtained under the flow conditions discussed earlier in connection with figure 2. The agreement seems quite satisfactory given that the scaling assumptions made in the asymptotic theory are not strictly met in the experiment.

6. Concluding remarks

Our analysis has confirmed that the three-dimensional propagation of internal gravity wave beams differs fundamentally from its two-dimensional counterpart. As also suggested by Bordes *et al.* (2012), three-dimensional variations trigger the transfer

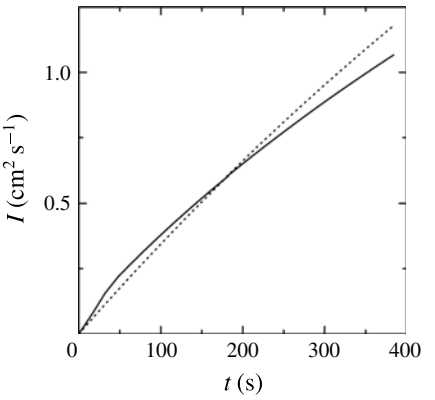

FIGURE 4. Temporal evolution of the integrated mean vertical vorticity $I(t)$ for the mean flow corresponding to the same flow conditions as in figure 2: solid line, theoretical prediction based on (5.3); dotted line, experimental results from Bordes *et al.* (2012).

of energy, through the action of Reynolds stresses, to a circulating horizontal mean flow. For a small-amplitude thin beam, this resonant beam–mean-flow interaction is described by a system of two evolution equations, namely (3.9) and (4.12) or (4.13), which also account for the feedback of the induced mean flow to the beam propagation. This relatively simple asymptotic model explains the salient features of the experimental observations of Bordes *et al.* (2012), most notably the jet-like behaviour of the induced mean flow in the beam interior, the transverse bending of the beam crests, as well as the temporal evolution of integrated mean vertical vorticity.

While the initial motivation for the present study came from the laboratory experiment of Bordes *et al.* (2012), the evolution equations derived here can be used to explore three-dimensional aspects of internal wave beams in other settings as well. For example, the far-field response to a concentrated line source with weak transverse dependence can be studied by putting

$$f(\eta, Z) = \hat{f}(Z)\delta(\eta), \tag{6.1}$$

rather than (5.1), on the right-hand side of (3.9). This choice of forcing would be appropriate for modelling the generation of wave beams by a long thin horizontal cylinder of slowly varying cross-section in the transverse direction, instead of the sinusoidal wave generator used in Bordes *et al.* (2012). In the case of a two-dimensional source ($\hat{f} = 1$), (3.9) admits a steady-state similarity solution (Thomas & Stevenson 1972), which corresponds to a propagating beam with locally confined profile that remains uniform in the transverse direction and is attenuated due to viscosity in the along-beam direction. When transverse (Z) variations are present, however, a steady state is no longer viable due to the generation of a growing mean flow, as indicated by (4.13). The long-time behaviour of the three-dimensional response, governed by the fully coupled system of (3.9) and (4.13), is currently an open question.

Finally, since uniform two-dimensional beams happen to be exact nonlinear states of the inviscid equations of motion (McEwan 1973; Tabaei & Akylas 2003), it appears that the weakly nonlinear theory developed here could be extended to thin beams of finite amplitude. Such a fully nonlinear model would be particularly useful

for examining the role of modulational instability, which arises above a certain threshold beam amplitude (Kataoka & Akylas 2013), in the long-time evolution of three-dimensional beams.

Acknowledgement

This work was supported in part by the US National Science Foundation under grant DMS-1107335.

REFERENCES

BORDES, G., VENAILLE, A., JOUBAUD, S., ODIER, P. & DAUXOIS, T. 2012 Experimental observation of a strong mean flow induced by internal gravity waves. *Phys. Fluids* **24**, 086602.

GOSTIAUX, L., DIDELLE, H., MERCIER, S. & DAUXOIS, T. 2007 A novel internal waves generator. *Exp. Fluids* **42**, 123–130.

GRISOUARD, N. & BÜHLER, O. 2012 Forcing of oceanic mean flows by dissipating internal tides. *J. Fluid Mech.* **708**, 250–278.

GRISOUARD, N., LECLAIR, M., GOSTIAUX, L. & STAQUET, C. 2013 Large scale energy transfer from an internal gravity wave reflecting on a simple slope. *Proc. IUTAM* **8**, 119–128.

KARIMI, H. H. & AKYLAS, T. R. 2014 Parametric subharmonic instability of internal waves: locally confined beams versus monochromatic wavetrains. *J. Fluid Mech.* **757**, 381–402.

KATAOKA, T. & AKYLAS, T. R. 2013 Stability of internal gravity wave beams to three-dimensional modulations. *J. Fluid Mech.* **736**, 67–90.

KOUDELLA, C. R. & STAQUET, C. 2006 Instability mechanisms of a two-dimensional progressive internal gravity wave. *J. Fluid Mech.* **548**, 165–196.

LIGHTHILL, M. J. 1978 *Waves in Fluids*. Cambridge University Press.

LIGHTHILL, M. J. 1996 Internal waves and related initial-value problems. *Dyn. Atmos. Oceans* **23**, 3–17.

MCEWAN, A. D. 1973 Interactions between internal gravity waves and their traumatic effect on a continuous stratification. *Boundary-Layer Meteorol.* **5**, 159–175.

MERCIER, M. J., MARTINAND, D., MATHUR, M., GOSTIAUX, L., PEACOCK, T. & DAUXOIS, T. 2010 New wave generation. *J. Fluid Mech.* **657**, 308–334.

MOWBRAY, D. E. & RARITY, B. S. H. 1967 A theoretical and experimental investigation of the phase configuration of internal waves of small amplitude in a density stratified fluid. *J. Fluid Mech.* **28**, 1–16.

STAQUET, C. & SOMMERIA, J. 2002 Internal gravity waves: from instabilities to turbulence. *Annu. Rev. Fluid Mech.* **34**, 559–593.

TABAEI, A. & AKYLAS, T. R. 2003 Nonlinear internal gravity wave beams. *J. Fluid Mech.* **482**, 141–161.

TABAEI, A. & AKYLAS, T. R. 2007 Resonant long–short wave interactions in an unbounded rotating stratified fluid. *Stud. Appl. Maths* **119**, 271–296.

THOMAS, N. H. & STEVENSON, T. N. 1972 A similarity solution for viscous internal waves. *J. Fluid Mech.* **54**, 495–506.